1988

Subsurface Stresses in Rolling/Sliding Machine Components

Farshid Sadeghi
Purdue University

Ping C. Sui
Purdue University

Follow this and additional works at: https://docs.lib.purdue.edu/icec

SUBSURFACE STRESSES IN ROLLING/SLIDING MACHINE COMPONENTS

Farshid Sadeghi
Assistant Professor

Ping C. Sui
Graduate Assistant

School of Mechanical Engineering, Purdue University, West Lafayette, IN 47907

ABSTRACT

The internal stress distribution in elastohydrodynamic lubrication of rolling/sliding line contact was obtained. The technique involves the full EHD solution and the use of Lagrangian quadrature to obtain the internal stress distributions in the x, y, z-directions and the shear stress distribution as a function of the normal pressure and the friction force. The principal stresses and the maximum shear stress were calculated for dimensionless loads ranging from (2.0452×10^{-5}) to (2.3×10^{-4}) and dimensionless velocity of 10^{-10} to 10^{-12} for slip ratios ranging from 0 to 100 percent.

INTRODUCTION

Machine components such as bearings, gears, cam and its followers, etc., are frequently subjected to high loads. The high load and high speed application of lubricated rolling/sliding contacts in which the elements elastically deform (elastohydrodynamic) has significant effect on the internal stress distributions in the elements. The fatigue life of heavily loaded rolling/sliding machine components are directly related to the stress distributions in the elements, assuming elastic and homogeneous material. The stress distributions for dry contacts are readily available [1]. However, in elastohydrodynamic lubrication, a film is formed between the elements separating their surfaces. The film thickness modifies the pressure and the internal stress distributions of the rolling/sliding elements. The interface of rolling/sliding elements supports the load while allowing the relative motion inherent in the mechanism to take place.

Hertz [2] was the first to investigate the stress distributions in dry contact. Thomas and Hoersch [3] in 1930 calculated stresses for varying depths below the contact surface of two spheres. Foeppl [4] in 1936 presented a solution to the problem of a cylinder and a spherical ball on a flat plate, and verified the results by photoelastic experiments. Lundberg and Palmgren [5] in 1947 developed the fundamental theory for rolling contact fatigue. This theory is based on the assumption that failure is in the form of shallow pitting and is related to subsurface shearing stresses in the rolling elements. Poritsky [6] in 1949 presented a solution to stresses due to tangential and normal loads on an elastic solid. He used a coefficient of friction of 0.3 in his analysis. Smith and Liu [7] in 1952 also presented results for stresses due to tangential and normal loads. They used a coefficient of friction of 1/3 and extended their analysis to study the significance of these stresses in causing failure by inelastic yielding and fatigue. Dowson, Higginson, and Whitaker [8] in 1963, studied the stress distribution in lubricated rolling contacts. However, the load considered was extremely low and traction force was neglected. Hamilton and Goodman [9] in 1966 developed a theory for circular sliding contacts. They presented a series of graphs for predicting friction effects for the circular contact. Bryant [10] presented a closed form solution for the stresses in crowned cylinders based on the Hertzian pressure distribution for the normal pressure and surface shear stress. Kannel and Tevaarwerk [11] in 1983 evaluated subsurface stresses under rolling/sliding contacts. However, they use the Hertzian pressure distribution to calculate the internal stress distributions.

Even though these references addressed the internal stresses problem, a solution which is based on the full EHD solution with the rolling/sliding forces included has not been developed. In the present analysis, a numerical solution to the problem of internal stresses in EHD lubrication of rolling/sliding contacts is obtained. The Reynolds and elasticity equations are simultaneously solved using the Newton-Raphson method developed by Okamura [12] and further modified by Houpert and Hamrock [13] to obtain the pressure distribution. The pressure distribution is used to obtain the sliding friction force, coefficient of friction, and shear stress on the surface. The pressure distribution and surface shear stress are then used to obtain subsurface normal and shear stress distributions. Stress invariants are employed to obtain the principal normal stresses and the maximum shear stress distributions.

LIST OF SYMBOLS

b   Half Hertzian length, $R(8W/\pi)^{1/2}$, m
D_{ij} Influence coefficient used to calculate elastic deformation at node i due to P_j
E   Young's modulus, Pa

E'	Equivalent Young's modulus $1/E' = 1/2\,((1-\nu_a^2)/E_a + (1-\nu_b^2)/E_b)$, Pa
f_T	Traction coefficient
G	Material parameter, $\alpha E'$
H	Dimensionless film thickness, hR/b^2
H_e	Dimensionless film thickness where $dP/dX = 0$
H_o	Dimensionless constant used in calculation of H
h	Film thickness, m
P	Dimensionless Pressure p/P_H
p	pressure, Pa
P_H	Maximum Hertzian pressure, $E'(W/2\pi)^{1/2}$, Pa
R	Equivalent radius of the contact, $1/R = 1/R_a + 1/R_b$,m
U	Dimensionless velocity (speed) parameter, $\mu_o u/E'R$
U_d	Dimensionless sliding velocity, $u_a - u_b/u$
u	Average rolling velocity $((u_a + u_b)/2)$,m/s
W	Dimensionless load parameter, $w/E'R$
w	Applied load per unit length, N/m
X	Dimensionless depth along the rolling direction , x/b
X_{end}	Outlet position
X_{min}	Inlet position
X'	Dummy variable
x	Coordinate along the rolling direction, m
Y	Dimensionless depth into the solid, y/b
y	Depth into the solid, m
z	Exponent for Roelands' viscosity model
α	Pressure viscosity exponent, m^2/N
$\bar{\mu}_i$	Dimensionless viscosity of the lubricant
μ_o	Ambient viscosity of the lubricant, Ns/m^2
$\bar{\rho}$	Relative density
$\bar{\rho}_e$	Relative density where $H = H_e$
$\bar{\rho}_i$	Dimensionless density
$\bar{\sigma}_x$	Normal stress in the rolling direction, Pa
σ_x	Dimensionless normal stress in the rolling direction, $\bar{\sigma}_x/P_H$
$\bar{\sigma}_y$	Normal stress in the solid, Pa
σ_y	Dimensionless normal stress in the solid, $\bar{\sigma}_y/P_H$
τ_{max}	Dimensionless maximum shear stress
$\bar{\tau}_{xy}$	Shear stress, Pa
τ_{xy}	Dimensionless shear stress, $\bar{\tau}_{xy}/P_H$

THE GOVERNING EQUATIONS

The Reynolds Equation with the appropriate assumptions [13] could be written in the dimensionless form as:

$$H_i^3 \left(\frac{dP}{dX} \right)_i - \left(\frac{3}{4} \frac{\pi^2 U}{W^2} \right) \bar{\mu}_i \left(H_i - \frac{\rho_e H_e}{\rho_i} \right) = 0 \tag{1}$$

where the boundary conditions are $P_1 = 0$ for $X_1 = X_{min}$ and $P = dP/dX = 0$ for $X = X_{end}$. The constant load condition is:

$$\int_{X_{min}}^{X_{end}} P\,dX = \frac{\pi}{2} \tag{2}$$

The film shape in the dimensionless form is given by [13];

where
$$H_i = H_o + \frac{X_i^2}{2} + \sum_{j=1}^{N} D_{ij} P_j \tag{3}$$

$$\sum_{j=1}^{N} D_{ij} P_j = -\frac{1}{2\pi} \int_{X_{min}}^{X_{end}} \frac{dP}{dX'} (X - X') \left[\ln(X - X')^2 - 2 \right] dX' \tag{4}$$

and H_o contains the term $-.25 \ln \left(\frac{8WR^2}{\pi} \right)$

630

The viscosity/pressure relationship used in this analysis was proposed by Roelands [14]. The Roelands equation in dimensionless form is;

$$\bar{\mu}_i = \exp\left\{\left[\ln(\mu_o) + 9.67\right]\left[-1 + \left(1 + 5.1 \times 10^{-9}P_HP_i\right)^z\right]\right\}$$ (5)

The exponent z can be expressed in terms of α and μ_o as;

$$\alpha = 5.1 \times 10^{-9}z\left[\ln(\mu_o) + 9.67\right]$$ (6)

where $G = \alpha E'$.

The density/pressure relationship used by Dowson and Higginson [15] in the dimensionless form is employed in this analysis.

$$\bar{\rho}_i = 1 + \frac{0.6 \times 10^{-9}\ P_HP_i}{1 + 1.7 \times 10^{-9}\ P_HP_i}$$ (7)

STRESS EQUATIONS

A triaxial state of stress exists at the conjuction region of rolling/sliding contacts; and the solids in contact are in a condition of plane strain. The plane strain condition implies that the shear stresses $\tau_{yz} = \tau_{zx} = 0$. Rolling/sliding contacts transmit normal pressure and tangential traction due to friction. Figure 1 depicts an elastic half space loaded over $X_{min} < X < X_{end}$ by a normal pressure $P(X')$ and tangential traction $Q(X')$. The stress functions for the state of loading over the entire length can be written as [16];
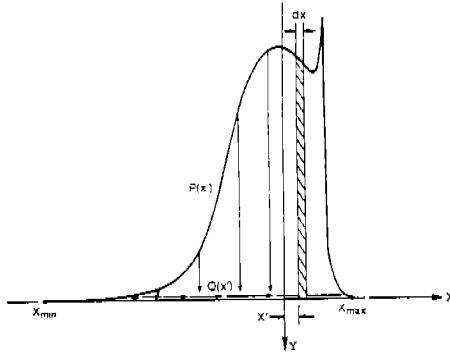

Figure 1. Pressure and traction distribution over an elastic half space.

$$\phi_P = -\frac{b^2}{\pi} \int_{X_{min}}^{X_{end}} P(X')(X - X') \tan^{-1}\left[\frac{X - X'}{Y}\right] dX'$$ (8)

$$\phi_r = -\frac{b^2}{\pi} Y \int_{X_{min}}^{X_{end}} Q(X') \tan^{-1}\left[\frac{Y}{X - X'}\right] dX'$$ (9)

Using these stress functions, the normal and shear stress distribution at any point inside the body resulting from the differential load and shear can be obtained.

$$\sigma_x = \frac{1}{b^2}\frac{\partial^2\phi}{\partial Y^2} = -\frac{2}{\pi}\left\{\int_{X_{min}}^{X_{end}} \frac{Y(X - X')^2}{\Lambda^4} P(X')dX' + \int_{X_{min}}^{X_{end}} \frac{(X - X')^3}{\Lambda^4} Q(X')dX'\right\}$$ (10)

$$\sigma_y = \frac{1}{b^2}\frac{\partial^2\phi}{\partial X^2} = -\frac{2}{\pi}\left\{\int_{X_{min}}^{X_{end}} \frac{Y^3}{\Lambda^4} P(X')dX' + \int_{X_{min}}^{X_{end}} \frac{Y^2(X - X')}{\Lambda^4} Q(X') dX'\right\}$$ (11)

$$\tau_{xy} = -\frac{1}{b^2}\frac{\partial^2\phi}{\partial X\partial Y} = -\frac{2}{\pi}\left\{\int_{X_{min}}^{X_{end}}\frac{Y^2(X-X')}{\Lambda^4}P(X')dX' + \int_{X_{min}}^{X_{end}}\frac{Y(X-X')^2}{\Lambda^4}Q(X')dX'\right\}$$ (12)

Where

$$\Lambda = \left[(X-X')^2 + Y^2\right]^{1/2}$$ (13)

with the boundary conditions given as [16];

$$\sigma_x(X,0) = -P(X) - \frac{2}{\pi}\int_{X_{min}}^{X_{end}}\frac{Q(X')}{(X-X')}dX'$$ (14)

$$\sigma_y(X,0) = -P(X)$$ (15)

$$\tau_{xy}(X,0) = \frac{U}{H}(\frac{\pi}{W})^{3/2}\frac{\bar{\mu}U_d}{\sqrt{32}} - H\ (\frac{2W}{\pi})^{1/2}\frac{dP}{dX}$$ (16)

Using equations (10) through (16) the subsurface normal stresses and shearing stress at any point in an EHD lubrication of rolling/sliding contact can be obtained. These stresses were used to obtain the stress invariants and principal stresses. The principal stresses are employed to obtain the maximum shear stress in the rolling/sliding elements. The maximum shear stress is given by:

$$\tau_{max} = \frac{1}{2}(\sigma_{max} - \sigma_{min}).$$ (17)

RESULTS AND DISCUSSION

Figures 2 through 5 illustrate the pressure and film thickness for dimensionless loads of $W = 2.0452 \times 10^{-5}$ to 2.3×10^{-4} and dimensionless velocity ranging from $U = 10^{-10}$ to 10^{-12} at material parameter $G = 5007$. The fast approach Newton-Raphson technique [13] was employed to solve the simultaneous system of Reynolds and elasticity equations. Figure 2 depicts that the pressure spike occurs at $X = .44$ from the center of the contact for $W = 2.0452 \times 10^{-5}$ and $U = 10^{-10}$. However, as the speed is decreased (Figure 2), the magnitude of the pressure spike decreases and the point of maximum pressure, where $dP/dX = 0$ occurs near the center of the contact. This condition also occurs as the load is increased for a constant velocity. A comparison of pressure profiles in Figures 2 and 3 for a constant velocity of $U = 10^{-11}$ reveals this fact. The points of maximum pressure and pressure spike are important since they significantly effect the surface shear stress. Figures 6 through 15 illustrate the contour plots of maximum shear stress distributions for the dimensionless velocity varying from $U = 10^{-10}$ to 10^{-12} and loads from $W = 2.0452 \times 10^{-5}$ to 2.3×10^{-4} for pure rolling and slip conditions.

Figure 6 illustrates the maximum shear stress distribution for the load $W = 2.0452 \times 10^{-5}$ and speed $U = 10^{-10}$ under pure rolling condition. Figure 6 depicts that the maximum shear stress reaches its maximum of 0.491 at the surface of the element and a point of stress concentration appears at the pressure spike. Figure 7a illustrates the maximum shear stress distributions at the same load and slip as in Figure 6 at the lower velocity of $U = 10^{-11}$. In this case the maximum shear stress reaches its maximum of 0.290 at 0.680 below the surface. However, as the slip is increased, the maximum shear stress moves towards the surface. An examination of Figure 7b indicates that at this load and speed the maximum shear stress of 0.343 occurs on the surface for 20 percent slip. Figure 8 elucidates the maximum shear stress contour for the load $W = 2.0452 \times 10^{-5}$ and speed $U = 10^{-12}$ under pure rolling and 100 percent slip conditions. Figure 8b indicates that for this load and velocity at 100 percent slip the maximum shear stress has moved towards the surface. However, it fails to reach the surface. The maximum shear stress reaches its maximum of 0.295 at 0.780 below the surface for pure rolling (Figure 8a) and at 0.660 below the surface for 100 percent slip condition (Figure 8b). Figure 9 depicts the maximum shear stress distribution at the pressure spike and the point of maximum pressure where $dP/dX = 0$. These points are of interest since they significantly effect the location of maximum shear stress. Figure 9a illustrates that at the point of maximum pressure $(dP/dX = 0)$, maximum shear stress occurs on the surface for 60% slip. Figure 9b depicts that τ_{max} is significantly higher at the pressure spike than at the point of maximum pressure $(dP/dX = 0)$. The magnitude of the shear stress is gradually reduced moving towards the interior of the solid.

Figure 10 through 12 illustrate the contours of maximum shear stress at the load $W = 7.0 \times 10^{-5}$ for velocities ranging from $U = 10^{-10}$ to 10^{-12} and variable slip ratios. Figure 10a illustrates the maximum shear stress distribution at the high speed of $U = 10^{-10}$ under pure rolling condition. For this load and velocity (Figure 10a), the maximum shear stress is 0.281 and occurs at 0.780 below the surface of the element. Comparing Figures 2 and 3 indicates that as the load was increased for a constant speed the magnitude of the pressure spike decreased. Hence, the maximum shear stress occurred below

the surface (Figure 10). However, at this load and speed a small amount of slip significantly effects the depth at which the maximum shear stress occurs (Figure 10b). Figure 10b illustrates that at 0.6 percent slip the maximum shear stress of 0.323 occurs at the surface. An examination of Figure 10b indicates that a region of maximum shear stress appears to be at a depth of 0.40 below the surface near the pressure spike region. However, closer examination of Figure 10b reveals that the maximum shear stress occurs on the surface near the point of maximum pressure. Similar observations can be made for the same load but at lower velocities. Figures 11 and 12 indicate that, at the lower speeds the slip has to be significantly increased for the maximum shear stress to move towards the surface.

Figures 13 through 15 are the contours for 2.3×10^{-4} load at speeds ranging from $U = 10^{-10}$ to 10^{-12} under pure rolling and slip conditions. For this high load under pure rolling condition (Figure 13a), the shear stress reaches its maximum of 0.294 at 0.780 below the surface. For 3×10^{-4} percent slip the maximum shear stress is 0.314 and occurs on the surface. For the same load at lower speed of $U = 10^{-11}$ (Figure 14), the maximum shear is 0.299 and occurs at 0.780 below the surface under pure rolling condition (Figure 14a) and 0.313 on the surface for 4×10^{-4} percent slip. Figure 15 illustrates the shear stress contour for the 10^{-12} speed case. The figure illustrates that the maximum shear stress occurs at 0.780 below the surface under pure rolling and moves to the surface for 6×10^{-4} percent slip.
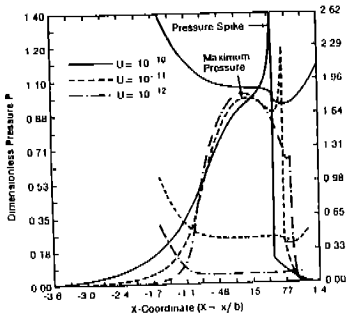
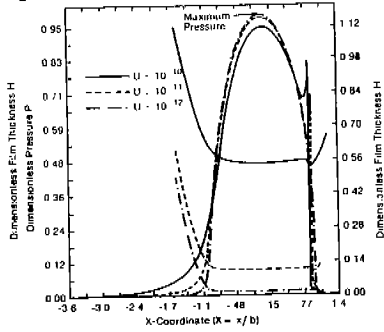Figure 2. Dimensionless pressure and film thickness for $W = 2.045 \times 10^{-4}$ and $G = 5007$.

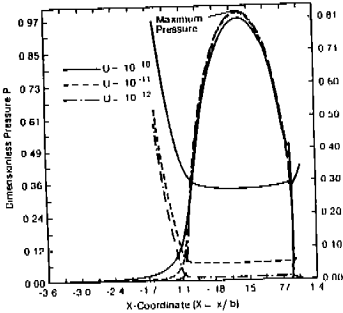Figure 3. Dimensionless pressure and film thickness for $W = 7.0 \times 10^{-4}$ and $G = 5007$.

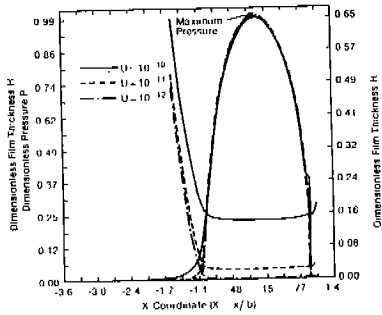Figure 4. Dimensionless pressure and film thickness for $W = 1.5 \times 10^{-4}$ and $G = 5007$.

Figure 5. Dimensionless pressure and film thickness for $W = 2.3 \times 10^{-4}$ and $G = 5007$.
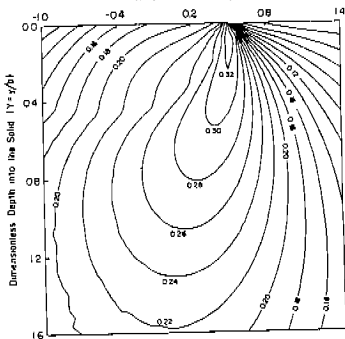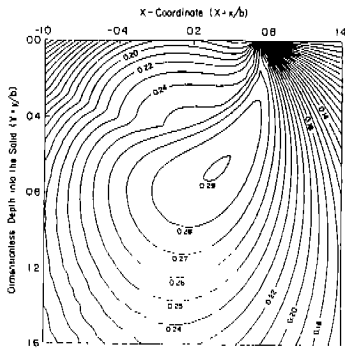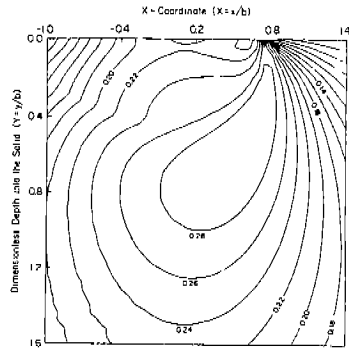

Figure 6. Dimensionless maximum shear stress contours for $W = 2.045 \times 10^{-4}$ $U = 1 \times 10^{-10}$ under pure rolling condition.
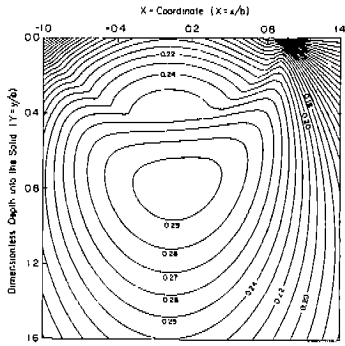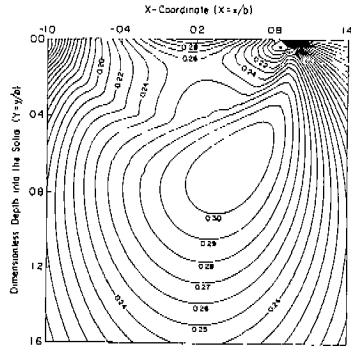
633

(a) pure rolling condition   (b) 20% slip condition

Figure 7.   Dimensionless maximum shear stress contours for W = 2.0452 x 10⁻⁶ and U = 1 x 10⁻¹¹.
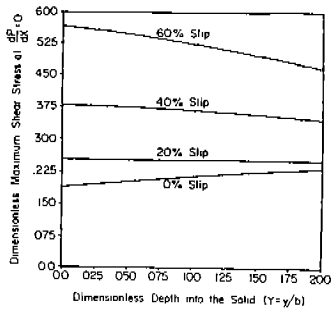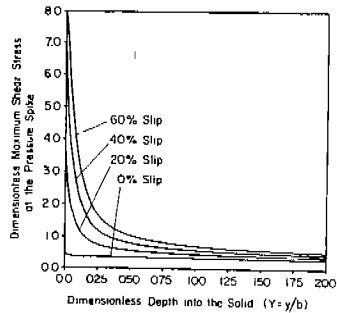

(a) pure rolling condition   (b) 100% slip condition

Figure 8.   Dimensionless maximum shear stress contours for W = 2.0452 x 10⁻⁶ and U = 1 x 10⁻¹².
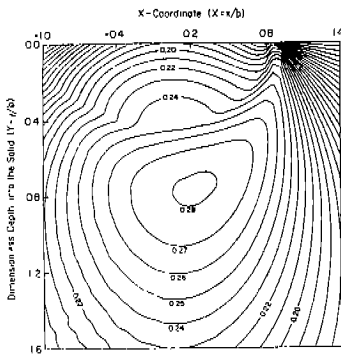

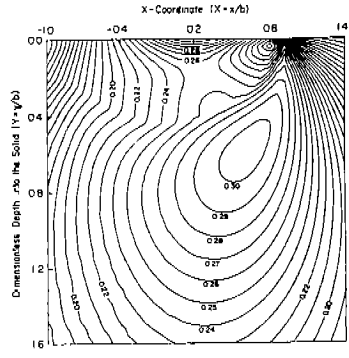(a) at the maximum pressure   (b) at the pressure spike

Figure 9.   Dimensionless maximum shear stress distribution in the solid at different slip conditions, W = 2.0452 x 10⁻⁶ and U = 1 x 10⁻¹⁰.
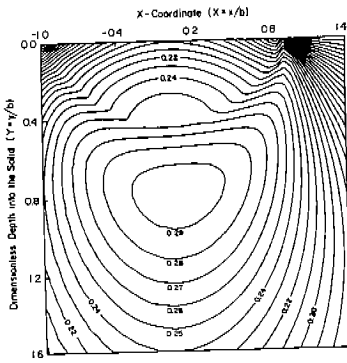
634

(a) pure rolling condition

(b) 0.5% slip condition

Figure 10. Dimensionless maximum shear stress contours for $W = 7.0 \times 10^{-5}$ and $U = 1 \times 10^{-10}$.

(a) pure rolling condition
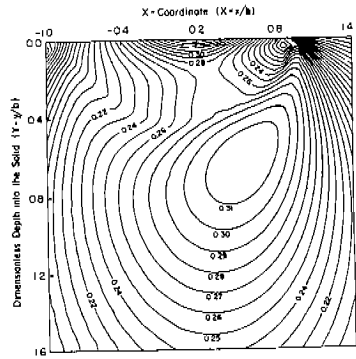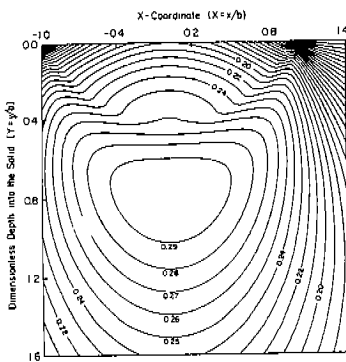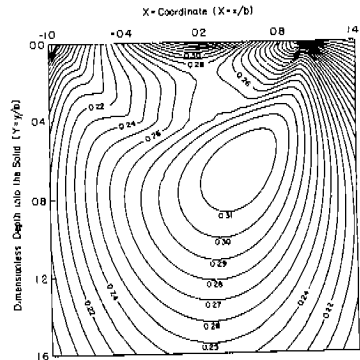
(b) 0.5% slip condition

Figure 11. Dimensionless maximum shear stress contours for $W = 7.0 \times 10^{-5}$ and $U = 1 \times 10^{-11}$.
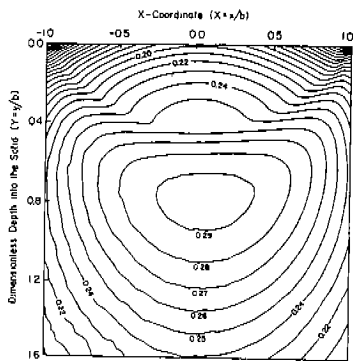

(a) pure rolling condition

(b) 1% slip condition

Figure 12. Dimensionless maximum shear stress contours for $W = 7.0 \times 10^{-5}$ and $U = 1 \times 10^{-12}$.

635

(a) pure rolling condition

(b) $3 \times 10^{-4}\%$ slip condition

Figure 13. Dimensionless maximum shear stress contours for $W = 2.3 \times 10^{-4}$ and $U = 1 \times 10^{-10}$.

(a) pure rolling condition

(b) $4 \times 10^{-4}\%$ slip condition

Figure 14. Dimensionless maximum shear stress contours for $W = 2.3 \times 10^{-4}$ and $U = 1 \times 10^{-11}$.
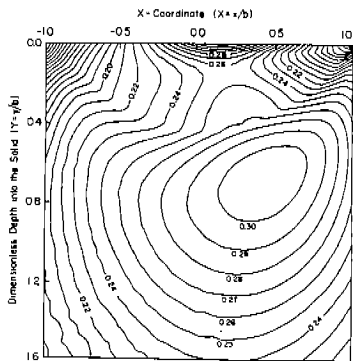

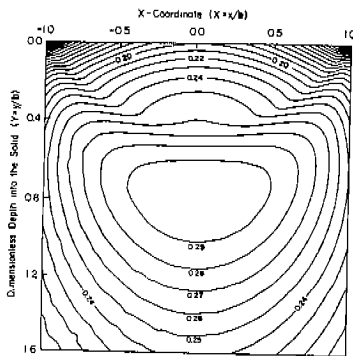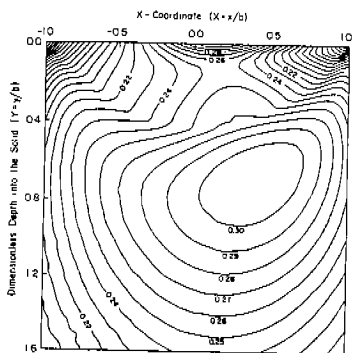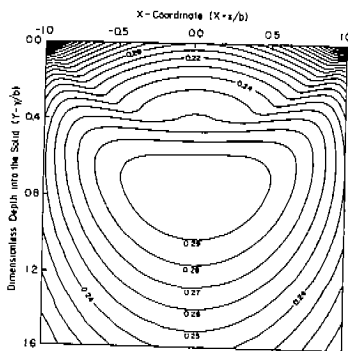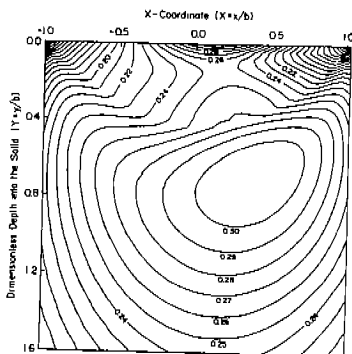
(a) pure rolling condition

(b) $5 \times 10^{-4}\%$ slip condition

Figure 15. Dimensionless maximum shear stress contours for $W = 2.3 \times 10^{-4}$ and $U = 1 \times 10^{-12}$.

636

Tables 1 and 2 contain the maximum shear stress and its location for different loads and velocities under pure rolling and slip conditions. Table 1 indicates that under pure rolling conditions the maximum shear stress for high loads occurs at 0.78 below the surface and near the center of the contact. However, at low loads and high speeds the maximum shear stress occurs closer to the surface and moves towards the exit zone. Table 2 contains the maximum shear stress under slip conditions obtained from the present method (Lagrange Quadrature Method, LQM) and the result of Smith [7]. The coefficient of friction for each loading, speed, and slip condition obtained from the LQM is presented in Table 2. The coefficient of friction for each condition was used to obtain the maximum shear stress for Smith's [7] analysis. A comparison of the maximum shear stresses in Table 2 indicates that, τ_{max} obtained from the LQM is significantly higher (19%) at low loads and high speeds. However, the error is reduced as the load is increased. The LQM indicates that, τ_{max} occurs on the surface for all loads, speeds, and slip conditions examined except for the lowest load and speed. However, Smith's Method [7] indicates that, τ_{max} always occurs below the surface for the examined conditions. The method developed represents a more accurate description of rolling/sliding contacts, since it simultaneously solves the Reynolds and elasticity equations to obtain the pressure profile and the stress distributions in the elements.

Table 1. Maximum shear stress and its location under pure rolling conditions.

W x 10^5	U x 10^{12}	X LQM	Y LQM	τ_{max} LQM
2.0452	100	0.520	0.000	0.491
	10	0.360	0.680	0.291
	1	0.295	0.780	0.295
7.0	100	0.240	0.780	0.281
	10	0.080	0.780	0.298
	1	0.000	0.780	0.299
13.0	100	0.120	0.780	0.290
	10	0.020	0.780	0.298
	1	0.000	0.780	0.300
23.0	100	0.075	0.780	0.294
	10	0.000	0.780	0.299
	1	0.000	0.780	0.300

Table 2. Maximum shear stress and its location under slip conditions.

W x 10^5	U x 10^{12}	% slip	f_T	X LQM	Y LQM	X [7]	Y [7]	τ_{max} LQM	τ_{max} [7]
2.0452	100	0	32×10^{-4}	0.52	0.0	0.00	0.78	0.491	0.300
	10	20	41×10^{-5}	0.74	0.0	0.14	0.78	0.343	0.301
	1	100	11×10^{-2}	0.50	0.66	0.36	0.72	0.310	0.306
7.0	100	6×10^{-1}	12×10^{-2}	0.18	0.0	0.40	0.72	0.323	0.306
	10	8×10^{-1}	15×10^{-2}	0.18	0.0	0.40	0.72	0.382	0.309
	1	1	14×10^{-2}	0.16	0.0	0.40	0.72	0.357	0.309
13.0	100	14×10^{-3}	95×10^{-3}	0.16	0.0	0.34	0.74	0.318	0.304
	10	16×10^{-3}	87×10^{-3}	0.14	0.0	0.28	0.74	0.310	0.304
	1	4×10^{-2}	10×10^{-2}	0.14	0.0	0.34	0.72	0.333	0.305
23.0	100	3×10^{-3}	82×10^{-3}	0.14	0.0	0.28	0.76	0.314	0.303
	10	4×10^{-4}	81×10^{-3}	0.14	0.0	0.28	0.76	0.313	0.303
	1	6×10^{-4}	79×10^{-3}	0.14	0.0	0.22	0.76	0.312	0.303

CONCLUSIONS

A solution to the problem of internal stress in elastohydrodynamic lubrication of rolling/sliding contacts is presented using the Newton-Raphson and Lagrangian quadrature method. For the highly idealized lubricant considered, the following conclusions were drawn:

1. Under pure rolling condition the maximum shear stress in general occurs at 0.780b below the surface.

2. Slip has significant effect on the depth at which the maximum shear stress occurs.

3. For low loads, the higher the speed, the closer to the surface the maximum shear stress occurs.

4. For high loads small amounts of slip draws the maximum shear stress to the surface.

5. The point of stress concentration occurs near the exit zone under low load conditions, however, as the load is increased this point moves toward the center of contact.

REFERENCES

1. Shigley, J.E., "Mechanical Engineering Design," Third Edition, McGraw Hill, 1977.
2. Morton, W.B., and Close, L.J., "Notes on Hertz Theory of the Contact of Elastic Bodies," Philosophical Magazine Series 6, Vol. 43, p. 320, 1922.
3. Thomas, H.R., and Hoersch, V.A., "Stresses Due to the Pressure of One Elastic Solid Upon Another," Univ. Ill., Engr. Expt. Sta., Bull. 212, 1930.
4. Foeppl, L., "Der Spannungszustand und die Austrengung des WerkStoffe, bei der Beruehrung Zweier Korper," Forschung auf dem Gebiek des Ingenienrwesens Ausgabe, A. Vol. 7, pp. 209-221, 1936.
5. Lundberg, G., and Palmgren, A., "Dynamic Capacity of Rolling Bearings," Ing. Vetanskap, Akad. - Handl., No. 196, 1947.
6. Poritsky, H., "Stresses and Deflections of Cylindrical Bodies in Contact with Application to Contact of Gears and Locomotive Wheels," *Journal of Applied Mechanics*, Trans. ASME, Vol. 72, pp. 191-201, 1950.
7. Smith, J.O., and Liu, C.K., "Stresses Due to Tangential and Normal Loads on an Elastic Solid With Application to Some Contact Stress Problems," *Journal of Applied Mechanics*, 1952.
8. Dowson, D., Higginson, G.R., and Whitaker, B.A., "Stress Distribution in Lubricated Rolling Contacts," Inst. Mech. Engrs., 1963.
9. Hamilton, G.H., and Goodman, C.E., "The Stress Field Created by Circular Sliding Contact," *ASME Journal of Applied Mechanics*, 1966.
10. Bryant, M.D., and Keer, L.J., "Rough Contact Between Elastically and Geometrically Identical Curved Bodies," *ASME Journal of Applied Mechanics*, Vol. 49, June 1982, pp. 345-359.
11. Kannel, J.W., Tevaarwerk, J.L., "Subsurface Stress Evaluations Under Rolling/Sliding Contacts," *Trans. of the ASME, ASLE,* Vol. 106, pp. 96-103, 1983.
12. Okamura, H., "A Contribution to the Numerical Analysis of Isothermal Elastohydrodynamic Lubrication," Tribology of Reciprocating Engines: *Proceedings of the 9th Leeds-Lyon Symposium on Tribology,* Butterworths, Guilford, England, pp. 313-320, 1982.
13. Houpert, L.G., and Hamrock, B.J., "Fast Approach for Calculating Film Thickness and Pressures in Elastohydrodynamic Lubricated Contacts at High Loads," *ASME Journal of Tribology,* Vol. 108, pp. 411-420, 1986.
14. Roelands, C.J.A., Vlugter, J.C., Watermann, H.I., "The Viscosity Temperature Pressure Relationship of Lubricating Oils and its Correlation with Chemical Constitution," *Journal of Basic Engineering,* pp. 601-606, 1963.
15. Dowson, D., Higginson, G.R., "Elastohydrodynamic Lubrication," Pergamon Press, 1966.
16. Kannel, J.W., Walowit, J.A., Bell, J.C., Allen, C.M., "The Determination of Stresses in Rolling Contact Elements," *ASME Journal of Lubrication Technology,* Vol. 89, pp. 483-467, 1967.